A Grid Search Algorithm to Determine Earthquake Source Parameters - Application to the 1992 Yellow Sea, China, Earthquake

John J. Cipar

DTIC
SELECTED
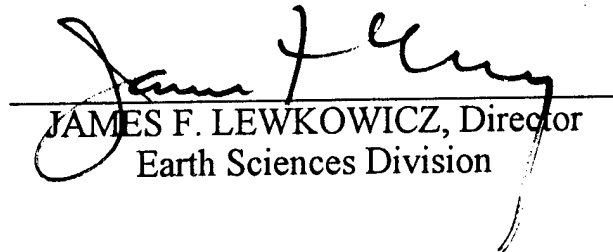DEC 0 8 1995
F

8 June 1995

19951206 052

PHILLIPS LABORATORY
Directorate of Geophysics
AIR FORCE MATERIEL COMMAND
HANSCOM AIR FORCE BASE, MA 01731-3010

This technical report has been reviewed and is approved for publication.

JAMES F. LEWKOWICZ, Director
Earth Sciences Division

This report has been reviewed by the ESC Public Affairs Office (PA) and is releasable to the National Technical Information Service (NTIS).

Qualified requestors may obtain additional copies from the Defense Technical Information Center (DTIC). All others should apply to the National Technical Information Service (NTIS).

REPORT DOCUMENTATION PAGE

1. AGENCY USE ONLY (Leave blank)	2. REPORT DATE 8 June 1995	3. REPORT TYPE AND DATES COVERED Scientific, Final

4. TITLE AND SUBTITLE
A Grid Search Algorithm to Determine Earthquake Source Parameters - Application to the 1992 Yellow Sea, China, Earthquake

5. FUNDING NUMBERS
PE61102F
2309G209

6. AUTHOR(S)
John J. Cipar

7. PERFORMING ORGANIZATION NAME(S) AND ADDRESS(ES)
Phillips Laboratory/GPE
29 Randolph Road
Hanscom AFB, MA 01731 - 3010

8. PERFORMING ORGANIZATION REPORT NUMBER
PL-TR-95-2082
ERP, No. 1171

9. SPONSORING/MONITORING AGENCY NAME(S) AND ADDRESS(ES)
AFSOR/NM
Bolling AFB, DC

10. SPONSORING/MONITORING AGENCY REPORT NUMBER

11. SUPPLEMENTARY NOTES

12a. DISTRIBUTION/AVAILABILITY STATEMENT
Approved for public release; distribution unlimited

12b. DISTRIBUTION CODE

13. ABSTRACT (Maximum 200 words)

A grid search method has been implemented to determine earthquake focal mechanism and source depth using a set of Green's functions computed for a representative continental crustal structure. The method directly compares observed and synthetic waveforms through a misfit function, selecting as the result the model with the lowest misfit. The method has been tested with synthetic data and with CDSN long-period (LH band) observations of the 1992 Yellow Sea earthquake. I obtain a focal mechanism and source depth broadly consistent with that inferred by Nguyen (1994): strike = 19^0, dip = 90^0, and rake = 173^0, depth = 15 km. Variations on the starting crustal model, which was derived from Nguyen and Hsu's (1993) MDJ model, are tested using the new focal mechanism. I find that better overall fits are obtained using higher attenuation throughout the crust and lower seismic velocity in the lower crust.

DTIC QUALITY INSPECTED 3

14. SUBJECT TERMS
Seismology, Earthquakes, Crustal structure, Korea

15. NUMBER OF PAGES
30

16. PRICE CODE

17. SECURITY CLASSIFICATION OF REPORT Unclassified	18. SECURITY CLASSIFICATION OF THIS PAGE Unclassified	19. SECURITY CLASSIFICATION OF ABSTRACT Unclassified	20. LIMITATION OF ABSTRACT SAR

Contents

Illustrations

Tables

Acknowledgments

A Grid Search Algorithm to Determine Earthquake Source Parameters – Application to the 1992 Yellow Sea, China, Earthquake

1. INTRODUCTION

In this report, I describe and test an algorithm for determining the focal mechanism, source depth, and seismic moment for an earthquake given a set of seismic waveform observations. The technique is based on the fact that a seismogram for an arbitrary focal mechanism is the linear combination of seismograms of three fundamental fault types. It is a straightforward task to create the Green's functions for these fundamental faults at a range of distances and source depths and to store them on computer disk. For a particular observed seismogram, the appropriate Green's functions are read from disk and combined to produce a trial synthetic. A misfit function is used to measure how closely the synthetic matches the observed seismogram. This is done for each seismogram in the data set. In the grid-search algorithm, this procedure is repeated for the entire range of focal mechanisms, and the mechanism with the lowest misfit is declared the winner. Separate inversion runs are done for each trial source depth, again selecting the lowest misfit as the correct depth.

The algorithm is tested by inverting a synthetic data set computed with a known mechanism and crustal model. A further test is done by using a synthetic data set created with a known mechanism and a radically different crustal model than the one used to compute the trial Green's functions. Finally, the algorithm is applied to a real data set:

1

Chinese Digital Seismograph Network (CDSN) observations of the November 3, 1992, Yellow Sea, China, earthquake.

Zhao and Helmberger (1994) have recently used this technique to invert for source parameters of earthquakes in California. They were fortunate enough to have detailed models of the crustal structure with which to compute the Green's functions for the inversion. Because of this, they could work with broadband (and inherently higher frequency) observations. In this paper, I will apply the method to the more common instance when the crustal structure is more poorly known and the Green's functions are, at best, approximations.

1.1 The 1992 Yellow Sea, China, Earthquake

A moderate earthquake occurred in the Yellow Sea region off the coast of eastern China on 3 November 1992 at 17h 31m 23.7s (UT). Coordinates are 35.328°N, 123.312°E; focal depth is 10 km, m_b = 4.8 (preceding information is from the Preliminary Determination of Epicenters, November, 1992, Monthly Listing). Figure 1 shows the earthquake location and the locations of the CDSN stations used in this study (Table 1). Each station recorded the data in three pass bands: long-period (LH), broad-band (BH), and short-period (SH) (Peterson and Tilgner, 1985). Nguyen (1994) used CDSN surface wave observations to determine the mechanism of the 1992 Yellow Sea earthquake to be nearly strike-slip with a minor amount of dip-slip. His mechanism, shown in Figure 1, is consistent with first-motion measurements observed on CDSN short-period records. The fault plane has the parameters: strike = 15°, dip = 80°, and rake = 155°. He determined the source depth and seismic moment to be 9 km and 8.42 x 10^{22} dyne-cm, respectively.

Table 1. CDSN Station Information

Station	Latitude (°N)	Longitude (°E)	Elevation (m)	Delta (deg)	Distance (km)	Azimuth (deg)	Back Azimuth (deg)	Location
BJI	40.0403	116.1750	43.0	7.357	817.958	311.860	127.490	Beijing
ENH	30.2800	109.4975	487.0	12.661	1408.070	250.471	62.954	Enshi
HIA	49.2667	119.7417	610.0	14.175	1575.558	350.415	167.994	Hailar
HKC	22.3036	114.1719	0.0	15.238	1694.948	214.049	29.608	Hong Kong
KMI	25.1500	102.7500	1952.0	20.421	2271.258	245.854	55.375	Kunming
LZH	36.0867	103.8444	1560.0	15.836	1760.627	278.427	86.992	Lanzhou
MDJ	44.6164	129.5919	250.00	10.449	1161.622	25.507	209.557	Mudanjiang
SSE	31.0956	121.1867	10.0	4.581	509.467	203.475	22.310	Sheshan
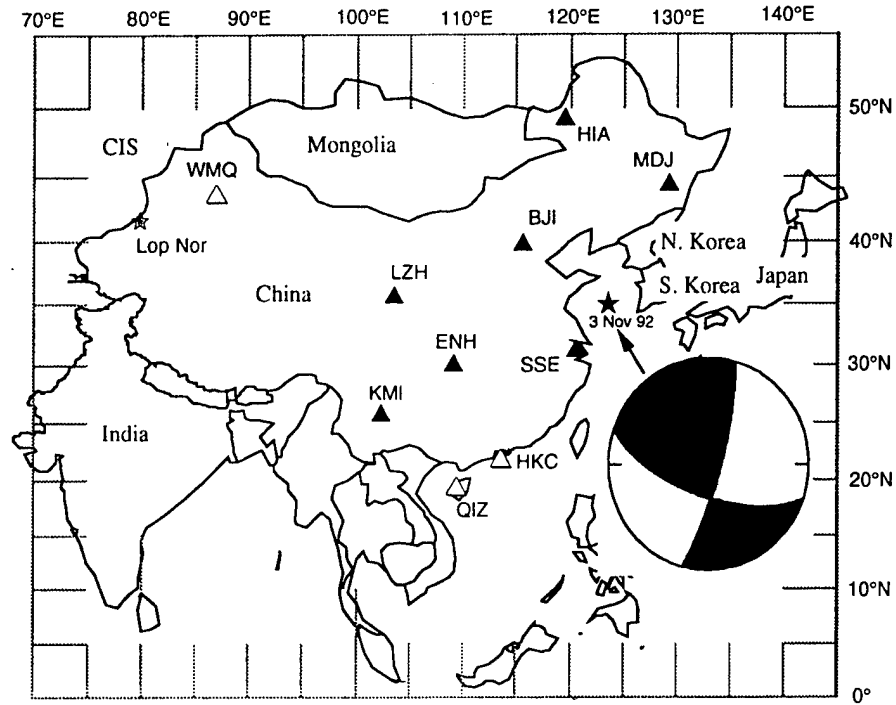
Figure 1. Map of the Location of the Yellow Sea Earthquake (Star) and the Stations (Triangles) Used in This Study. Open triangles denote other stations in the area. The inset shows the focal mechanism reported by Nguyen (1994); shaded quadrants are compressional.

1.2   Model for Crustal Structure

The starting velocity model for the crust was determined by Nguyen and Hsu (1993) as their MDJ model. The model was extended into the upper mantle using a constant velocity gradient. Although the attenuation was set rather high, the values are broadly consistent with previous measurements for the continental crust (Cheng and Mitchell, 1981). This starting model is designated A5 and is given in Table 2a.

Model A5 was tested by computing reflectivity synthetic seismograms and comparing these directly to the observed CDSN LH records (Figure 2). This combination of source and crustal model produces synthetics which agree in a general sense with the data, but which differ considerably in detail. While the transverse components fit quite well across the entire distance range, the vertical and radial components have much poorer fits. The motivation for this study is to develop a method to exhaustively search the focal mechanism space in order to find the source model which best fits the observed data. A further goal, as mentioned above, is to use the method not only in the case where the structure is well-known, but to assess its utility in cases where the structure is known only in a general sense.

3

Table 2. Crustal Models

Depth (km)	P-velocity (km/s)	Q_p	S-velocity (km/s)	Q_s	Density (g/cm^3)
(a) Model A5					
0.0	4.06	200.0000	2.3500	100.0000	2.3300
1.0	4.06	200.0000	2.3500	100.0000	2.3300
1.0	5.42	1000.0000	3.1300	500.0000	2.5800
3.0	5.42	1000.0000	3.1300	500.0000	2.5800
3.0	6.16	1000.0000	3.5600	500.0000	2.7500
16.0	6.16	1000.0000	3.5600	500.0000	2.7500
16.0	7.16	1000.0000	4.1400	500.0000	3.0300
40.0	7.16	1000.0000	4.1400	500.0000	3.0300
40.0	7.76	1000.0000	4.4800	500.0000	3.2300
70.0	8.10	1000.0000	4.6767	500.0000	3.3203
100.0	8.20	1000.0000	4.7344	500.0000	3.3582
130.0	8.40	1000.0000	4.8499	500.0000	3.4339
160.0	8.50	1000.0000	4.9076	500.0000	3.4718
(b) Model A7					
0.0	4.0600	50.0000	2.3500	25.0000	2.3300
1.0	4.0600	50.0000	2.3500	25.0000	2.3300
1.0	5.4200	100.0000	3.1300	50.0000	2.5800
3.0	5.4200	100.0000	3.1300	50.0000	2.5800
3.0	6.1600	525.0000	3.5600	263.0000	2.7500
16.0	6.1600	525.0000	3.5600	263.0000	2.7500
16.0	7.1600	525.0000	4.1400	263.0000	3.0300
40.0	7.1600	525.0000	4.1400	263.0000	3.0300
40.0	7.7600	525.0000	4.4800	263.0000	3.2300
70.0	8.1000	525.0000	4.6767	263.0000	3.3203
100.0	8.2000	525.0000	4.7344	263.0000	3.3582
130.0	8.4000	525.0000	4.8499	263.0000	3.4339
160.0	8.5000	525.0000	4.9076	263.0000	3.4718
(c) Model A8					
0.0	4.0600	50.0000	2.3500	25.0000	2.3300
1.0	4.0600	50.0000	2.3500	25.0000	2.3300
1.0	5.4200	100.0000	3.1300	50.0000	2.5800
3.0	5.4200	100.0000	3.1300	50.0000	2.5800
3.0	6.1600	525.0000	3.5600	263.0000	2.7500
16.0	6.1600	525.0000	3.5600	263.0000	2.7500
16.0	6.8000	525.0000	3.9261	263.0000	2.8278
40.0	6.8000	525.0000	3.9261	263.0000	2.8278
40.0	7.7600	525.0000	4.4800	263.0000	3.2300
70.0	8.1000	525.0000	4.6767	263.0000	3.3203
100.0	8.2000	525.0000	4.7344	263.0000	3.3582
130.0	8.4000	525.0000	4.8499	263.0000	3.4339
160.0	8.5000	525.0000	4.9076	263.0000	3.4718

2. GRID SEARCH ALGORITHM

The grid search algorithm used in this report is similar to the one described by Zhao and Helmberger (1994). The basic concept is that an earthquake waveform for any focal mechanism can be built up from a linear combination of three fundamental earthquake Green's functions: a strike-slip fault with a fault plane dipping 90°, a 90° dip-slip fault, and a 45° dip-slip fault. The fundamental Green's functions are weighted by expressions involving the fault strike, dip and rake, as well as the azimuth of the fault plane to the azimuth of the station (see Helmberger and Engen, 1980; Wallace *et al.*, 1981). In this report, I use Green's functions computed using the reflectivity method (Fuchs and Muller, 1971; Muller, 1985) and the fundamental Green's functions are related through the moment tensor.

Following Muller (1985), we can write the vertical or radial ground displacement (P-SV system) for a shear source in a layered medium as:

$$U_z = [I(t) * S(t) * Q(t)] * \sum_{i=1}^{3} k_i [G_z(t)] \tag{1}$$

where: $G_z(t)$ is the Green's function that depends on the layered crustal model;

$I(t)$ is the instrument operator;

$S(t)$ is the operator that describes the source time history;

$Q(t)$ is the operator that describes the attenuation structure.

The three k_is are weighting constants that depend on the elements of the moment tensor and the source orientation relative to the station. Another set of two constants describes the transverse motion (SH system). The formulas for these constants are given in Muller (1985).

In the practical implementation of the algorithm, each of the k_is are set to unity in turn with the other k_i set to zero. The resulting Green's functions for each case are computed and stored on disk. This is done in turn for each k_i and for the corresponding SH constants. To produce a synthetic, the Green's functions appropriate for the event depth and distance are retrieved from disk and weighted according to the k_i computed for the trial focal mechanism. These are summed to produce the synthetics.

2.1   Test Green's Functions

The Green's functions used in the inversion were computed every 50 km from 300 to 1850 km using the A5 model (Table 2). The program automatically selects the Green's function closest in distance to a given observation station. Green's functions were

5

computed for source depths between 6 and 18 km in steps of 3 km. A separate inversion was performed for each depth.

2.2 Fitness Functions

The data are compared to the synthetics by means of a "goodness-of-fit" or conversely, misfit function, of which several have been proposed. In this report, I use the normalized L_2 misfit function (Menke, 1984, p. 36-39) defined as:

$$L_2 = \sum_{j=1}^{N} \sum_{t=0}^{\infty} \frac{\left[x_j(t) - w_j(t)\right]^2}{\left[x_j^2(t)\right]}$$

(2)

where: $x_j(t)$ = the observed seismogram
$w_j(t)$ = the corresponding synthetic
N = the number of stations

YS-LH.INVERT (DATA:SOLID) - YS-A5.LH (SYNTHETIC:DASHED)
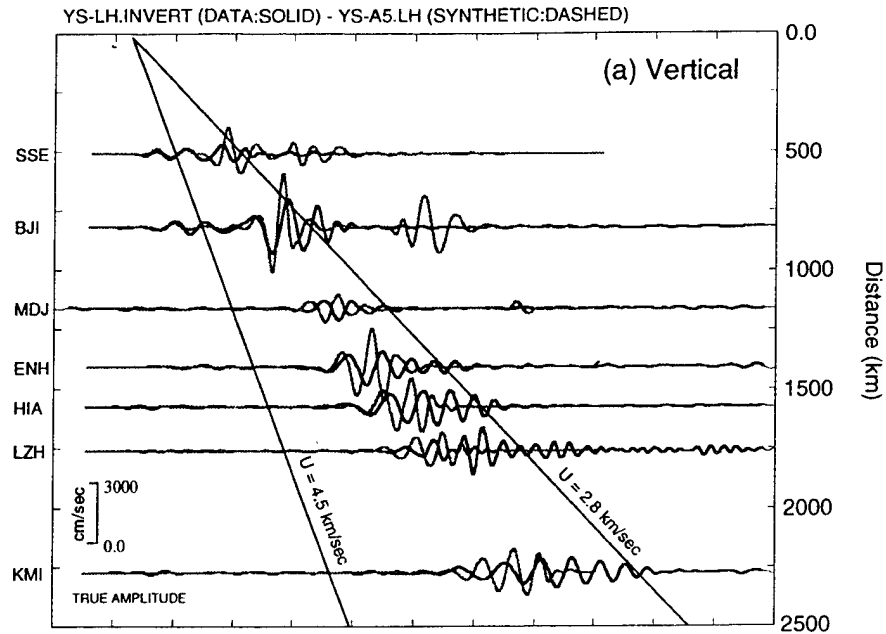
(a)

Figure 2. Vertical (a), Radial (b), and Transverse (c) Record Sections showing the Synthetics (Dashed Line) for Model A5 Computed With the Nguyen (1994) Source Parameters Compared With the Observed Data (Solid Line). The lines show the limits of the group velocity window between 4.5 and 2.8 km/sec.

6
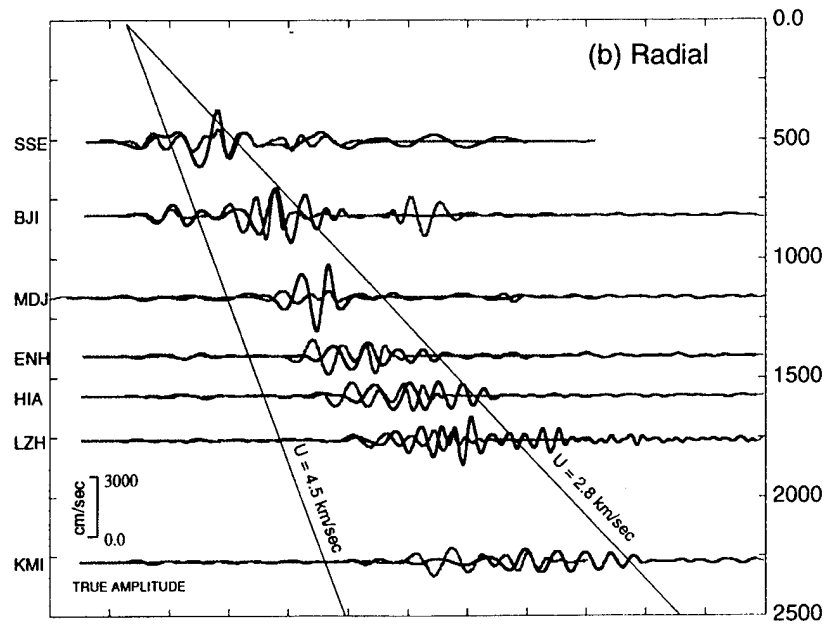
(b)
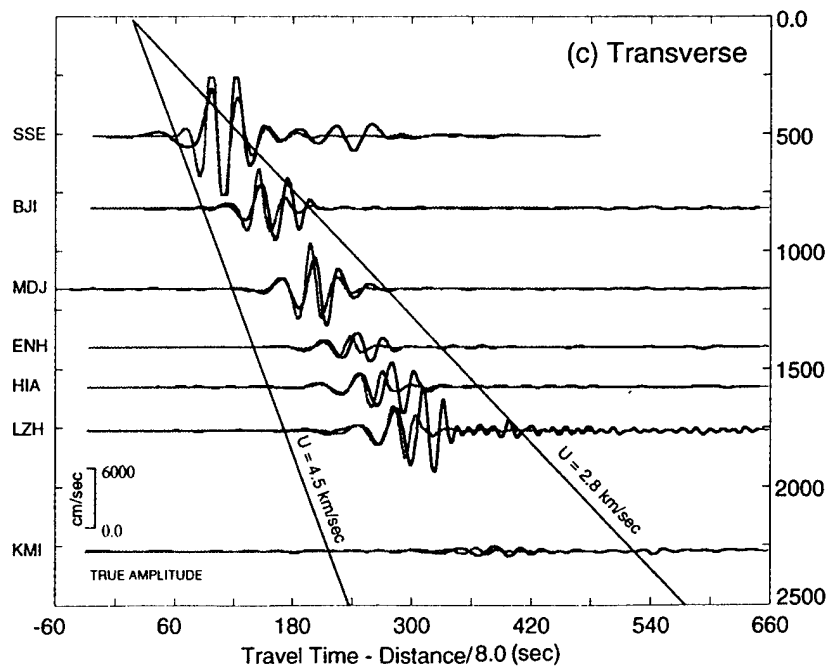
(c)

Figure 2. Vertical (a), Radial (b), and Transverse (c) Record Sections showing the Synthetics (Dashed Line) for Model A5 Computed With the Nguyen (1994) Source Parameters Compared With the Observed Data (Solid Line). The lines show the limits of the group velocity window between 4.5 and 2.8 km/sec.

7

2.3   Group Velocity Window Feature

The algorithm has a feature that allows the user to select a group velocity window for the calculations. In this way, different segments of the waveforms can be inverted separately. This feature ensures the same time segments of both the observed data and synthetics are being compared for the misfit calculations. This is particularly important because the data and synthetics may have quite different starting times.

2.4   Time Offset Feature

The observed data and synthetics are compared over a range of time offsets selected by the user. This feature allows for uncertainty in event location, which can produce time shifts between stations, as well as uncertainty in origin time which produces the same time shift at all stations. If the event location and origin time are sufficiently well known, the time offsets at each station can provide a measure of travel time residuals (see Zhao and Helmberger, 1994).

2.5   Amplitude Normalization Feature

Amplitudes of the synthetic seismograms are normalized to the observed amplitudes for all components by station. Individual station normalizations are averaged to determine the correct overall normalization for the event. It is this average normalization which is used to correct the synthetic waveforms to best match the observed. This procedure preserves the relative amplitudes between stations.

2.6   Instrument Response

I have taken the approach of convolving the synthetics with the measured instrument response and comparing these directly with the observed data. Doing this avoids the complications of deconvolving the instrument response from the observed data with the attendant problems of band-pass filtering and/or using an empirical water level to insure that the program does not amplify signals at the ends of the instrumental pass band. All of the synthetics shown in this paper have been computed using the MDJ LH instrument response as defined by the pole-zero file. Instrument responses were similar (<8% difference) at most stations for all components. The only exception was station LZH at which the normalization constant differed from the MDJ value by 25%.

3. TESTING THE ALGORITHM

The algorithm was tested by inverting a synthetic data set computed with a known focal mechanism and crustal structure. I used the mechanism determined by Nguyen (1994) for the Yellow Sea earthquake: strike=15°, dip = 80°, rake=155°, depth=9 km. The structure used for the test synthetics was model A5 (Table 2a). The results of the inversion are given in Table 3a. As expected, the error function is lowest for the source at 9 km depth and the algorithm correctly determined the mechanism at that depth. At other depths, the algorithm determined a slightly different mechanism, in accord with the experience reported by Zhao & Helmberger(1994). The synthetic "data" waveforms virtually overlie the results of the inversion, not surprising considering the small misfits. All of the misfit can be ascribed to the fact that the "data" were computed at the correct station distances, while the inversion synthetics were computed at the nearest multiple of 50 km. In the worst case, the data and synthetics have a 25-km difference in distance. The synthetic-observed time shifts for this case are all 0 to +/- 1 sec, again reflecting the distance differences and the fact that we are using the correct crustal model. It appears from this test that having Green's functions computed at 50-km intervals is sufficiently close for the source inversion.

A more rigorous test is provided by inverting for the focal mechanism using a set of synthetic "data" computed with a radically different crustal model. I chose the BJI-NW model derived by Mangino and Ebel (1992) using teleseismic receiver function observations at the CDSN station BJI. This model has a thick layer of low velocity material (6-6.1 km/sec) to 32 km depth. The velocity rises rapidly near the Moho which is at 40 km depth. This model is unusual in that it lacks the 6.5-7.1 km/sec, 10-20 km thick lower crustal layer found in most parts of the continents (Meissner, 1986) and as such is a good candidate for this test. Synthetic "data" were computed for the BJI-NW crustal model using Nguyen's (1994) focal mechanism at a source depth of 9 km. This data set was then inverted for depth and focal mechanism using the model A5 Green's functions. The misfits as a function of depth are given in Table 3b. The misfits are quite large and the inversion does not find the correct mechanism, although it gets reasonably close. The depth is estimated to be 15 km rather than the true depth of 9 km. The lesson of this exercise is that the method appears to work in determining the depth and focal mechanism, provided the crustal structure is reasonably well known.

4. TEST WITH REAL DATA: CDSN OBSERVATIONS OF THE YELLOW SEA EARTHQUAKE

In this report on the grid search algorithm, I decided to use the long-period (LH) channels at each CDSN station as the observed data set. The LH data should be less susceptible to scattering and slight changes in crustal structure. The data for CDSN stations SSE, MDJ, BJI, HIA, LZH, and ENH were rotated to radial and transverse,

9

detrended, and inverted for focal mechanism at trial source depths of 6, 9, 12, 15, and 18 km. The time offsets between observed and synthetic were allowed to vary by +/-10 sec. The results are shown in Figures 3, 4, and Table 3c. The L_2 norms for the best fitting mechanism are plotted as a function of depth in Figure 4. The closed stars show the misfits computed for a coarse grid spacing of 5°, that is, the strike, dip, and rake were incremented by 5° for each trial. The open star at 15 km is the misfit for an inversion run using a 1° increment over the mechanism range spanning the best coarse solution. For the real data, the best fitting depth is 15 km, 6 km deeper than the depth determined by Nguyen (1994). The inferred mechanism is slightly different as well with a strike = 19°, dip = 90°, and rake = 173°. This mechanism is broadly consistent with the results reported by Nguyen (1994) especially given the fact that this inversion did not use any constraints such as P-wave polarities. It should be noted, however, that the focal mechanism reported by Nguyen (1994) produced rather large misfits at all source depths. The inferred source depth, 15 km, is well within the depths expected for a continental earthquake.

Table 3. Inversion Results.

Depth	L_2 Misfit	Strike	Dip	Rake
(a) Model A5 with Nguyen source parameters				
6	0.08297	15	80	150
9	0.02926	15	80	155
12	0.06345	15	80	160
15	0.11269	15	85	165
18	0.74505	15	75	155
(b) Mangino BJI-NW model with Nguyen source				
6	2.57057	20	85	175
9	2.23688	20	90	175
12	2.02213	20	90	175
15	1.94190	20	90	180
18	2.67238	60	45	100
(c) Observed data with model A5 Green's functions				
6	1.36570	200	80	220
9	1.23418	200	85	195
12	1.10844	200	90	190
15	1.04025	200	90	185
15	1.04025	20	90	175
15*	**1.00050**	**19**	**90**	**173**
18	1.30252	10	70	140

The inversion synthetics are compared to the observed data in Figure 3. Note the considerable improvement compared to synthetics for model A5 (Figure 2), especially for the vertical components at SSE, BJI, ENH, and HIA. The transverse fits have remained very good, although the radial components still exhibit significant misfit. Overall, the relative amplitudes between stations are better as a result of tweaking the focal mechanism.


5. TESTS OF VARIATIONS IN THE CRUSTAL STRUCTURE MODEL

The focal mechanism inversion provides a source model that produces better overall agreement between observed and synthetic seismograms. Further improvement can be gained by modifying the crustal structure. It appears from Figure 3 that model A5 predicts seismograms that have higher overall frequencies than the data. To account for the higher attenuation of long-period surface waves, the Q values were reduced throughout the crust and upper mantle. The Q in the uppermost crust (the sediments) was reduced further to match the low Q values found in sediments. The resulting model, designated as A7, is given in Table 2b. Synthetics for model A7 computed using the focal mechanism and depth found by inversion had significantly smaller L_2 misfits compared to model A5: 2.02 for A5 compared to 1.56 for A7. Note that the L_2 misfits quoted in this section are computed with no synthetic-observed time shift. The data and synthetics are compared in Figure 5. The overall fit is improved compared to model A5, however the synthetics and observed are still out of phase (see, for example, the vertical components at stations ENH and HIA).

Next, I computed synthetics with various modifications of A7 to test how velocity changes at various depths within the structure affected the waveforms. The velocity in the lower crust of model A7 seemed somewhat high compared to other continental regions, especially in light of the relatively low upper mantle velocities. As a test, model A8 with lower crustal P-wave velocity reduced to 6.8 km/sec was computed (Table 2c). This model fit the best, with a misfit of 1.38, compared to 2.02 for A5 and 1.57 for A7. Other tests, such as increasing the upper mantle velocity, or changing the upper crustal velocity, produced synthetics with misfits larger than A7, although lower than A5. Vertical, radial, and transverse synthetics for model A8 are shown in Figure 6, along with the observed seismograms.
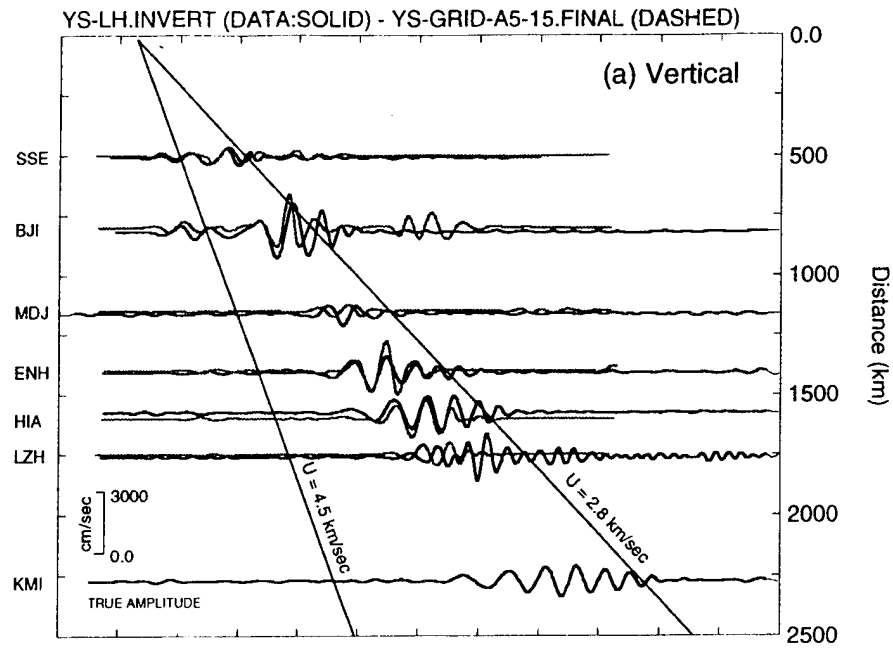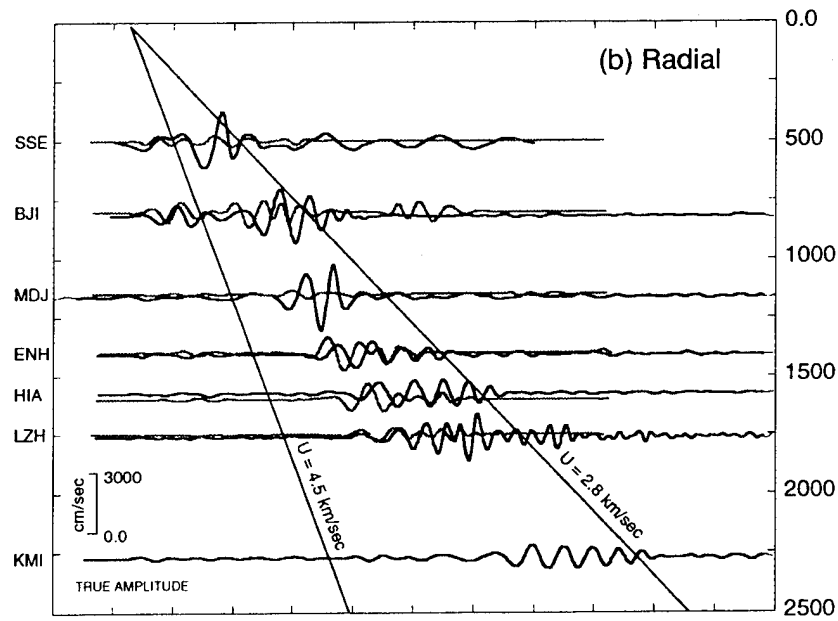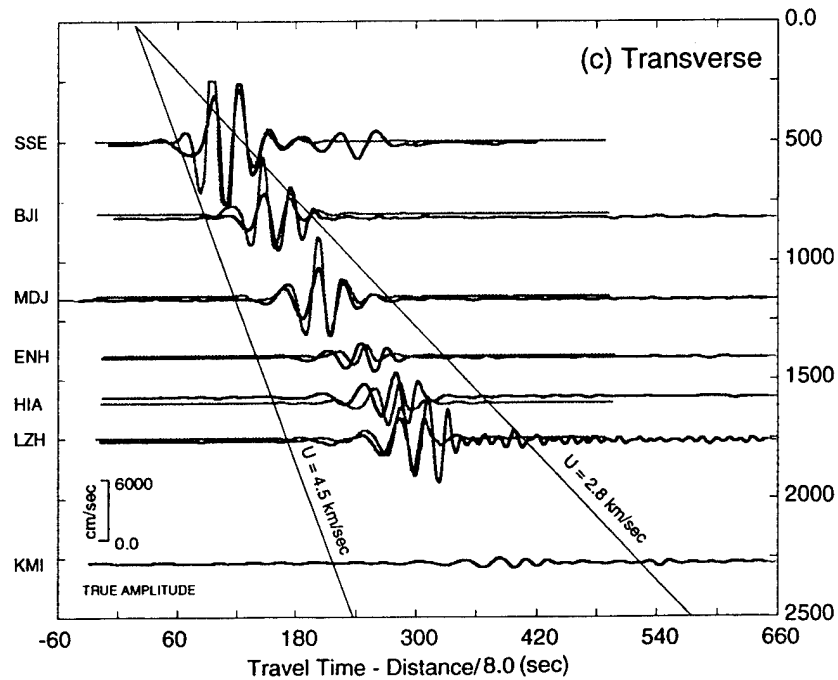
Figure 3. Vertical (a), Radial (b), and Transverse (c) Record Sections Showing the Final Inversion Synthetics (Dashed Line) Computed Using the Model A5 Green's Functions Compared With the Observed Data (Solid Line). The lines show the limits of the group velocity window between 4.5 and 2.8 km/sec.

(c)

Figure 3. Vertical (a), Radial (b), and Transverse (c) Record Sections Showing
the Final Inversion Synthetics (Dashed Line) Computed Using the Model A5
Green's Functions Compared With the Observed Data (Solid Line). The lines
show the limits of the group velocity window between 4.5 and 2.8 km/sec.

6. DISCUSSION

In this report, I have assumed that a single crustal model can be used to fit the
seismograms at all stations. This assumption is justified because the surface waves that
dominate the long-period observations have wavelengths between 30 and 130 km. Thus,
short wavelength perturbations in the crustal structure tend to be averaged out by this data
set. If higher frequency observations are used, these variations in crustal structure become
increasingly important. For example, Nguyen and Hsu (1993) derived different structures
for each CDSN station and Zhao and Helmberger (1994) obtained excellent fits between
synthetic and observed by determining a synthetic-to-observed time offset for each path.
These path-dependent time offsets imply different structures along each path. My approach
is to keep the crustal model as simple as possible until the data force adoption of a more
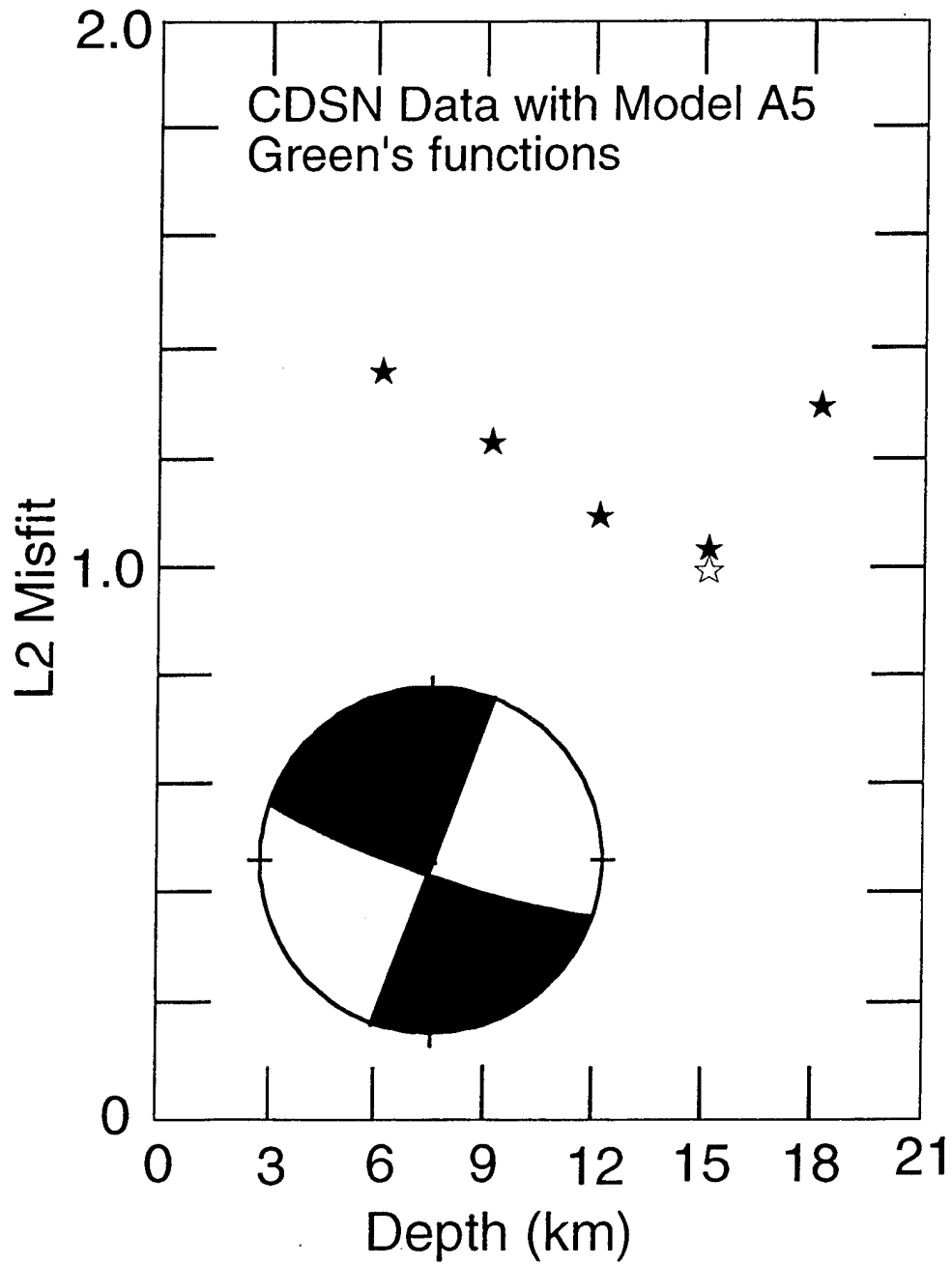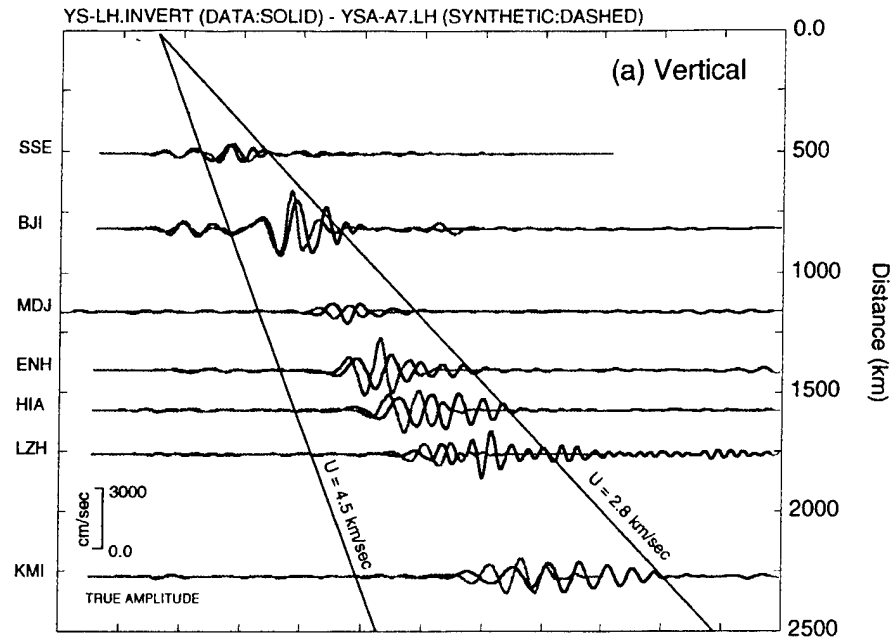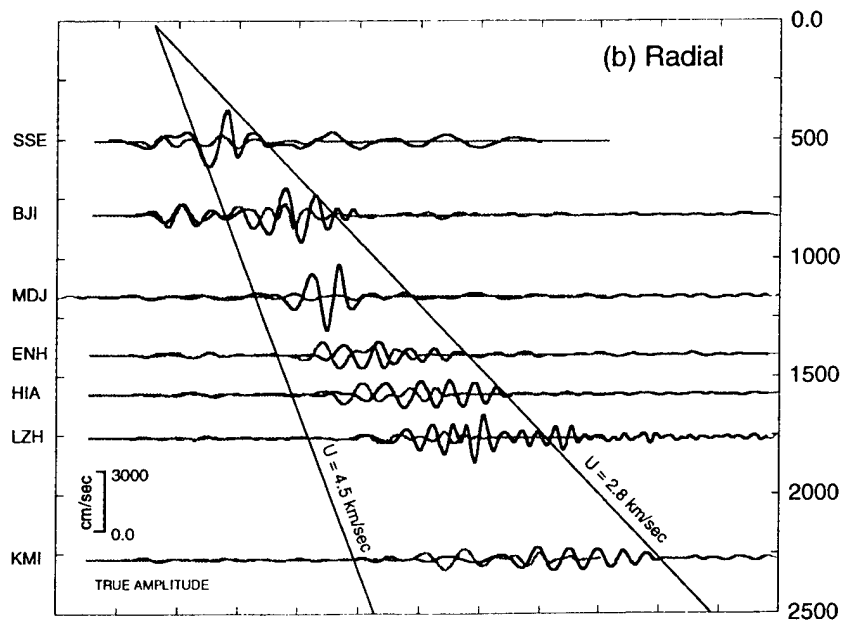complex structure.

13

Figure 4. L_2 Norms for the Observed Data Inverted Using the Green's Function for Model A5 as a Function of Depth. The best fitting focal mechanism at 15 km depth is shown in the inset; shaded quadrants are compressional.

It is clear from the preceding discussion that there is a trade-off between the source parameters and the crustal structure model. Clearly, the best approach is to fix one set of variables and invert for the other. For example, if the source is known from teleseismic observations, then the crustal structure can be derived from the regional waveforms. This is possible when several large events have been recorded simultaneously on regional and teleseismic stations (see Zhao and Helmberger, 1994). One of the drawbacks of the analog World-Wide Standardized Seismograph Network (WWSSN) was that an earthquake large enough to be seen at teleseismic distances invariably produced a signal that was clipped at regional stations. The recent advent of high dynamic range, broad-band digital instruments will alleviate this problem. Unfortunately, the Yellow Sea earthquake was not well recorded at teleseismic distances and thus a focal mechanism model derived independently of the regional data is not available. For this event, we have to bootstrap our understanding of both the focal mechanism and the regional structure.

YS-LH.INVERT (DATA:SOLID) - YSA-A7.LH (SYNTHETIC:DASHED)

(a) Vertical

SSE

BJI

MDJ

ENH

HIA

LZH

U = 4.5 km/sec

U = 2.8 km/sec

3000

cm/sec

0.0

TRUE AMPLITUDE

KMI

0.0

500

1000

Distance (km)

1500

2000

2500

(a)

(b) Radial

SSE

BJI

MDJ

ENH

HIA

LZH

U = 4.5 km/sec

U = 2.8 km/sec

3000

cm/sec

0.0

TRUE AMPLITUDE

KMI

0.0

500

1000

1500

2000

2500

(b)

Figure 5. Vertical (a), Radial (b), and Transverse (c) Record Sections Comparing Observed Data (Solid Line) With Model A7 Synthetics (Dashed Line). The lines show the limits of the group velocity window between 4.5 and 2.8 km/sec.
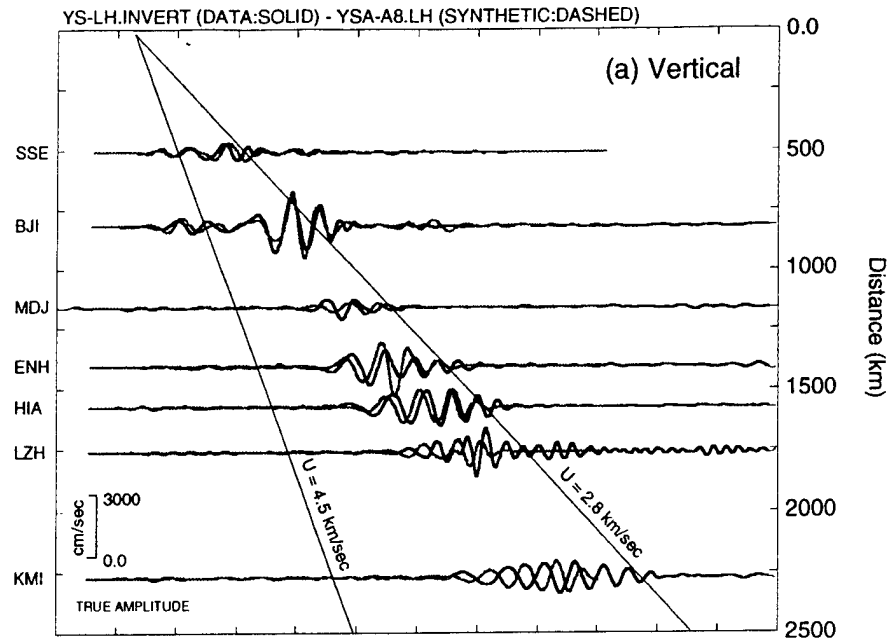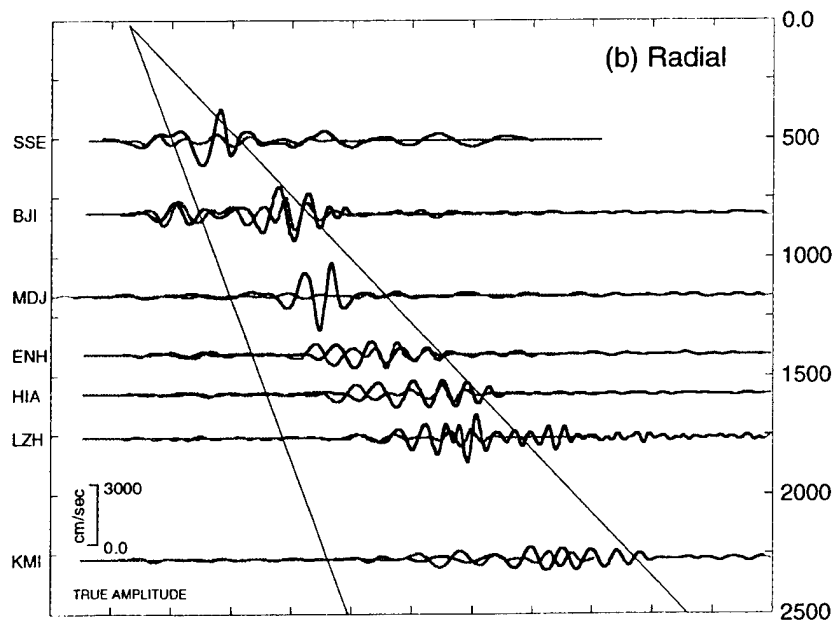
16
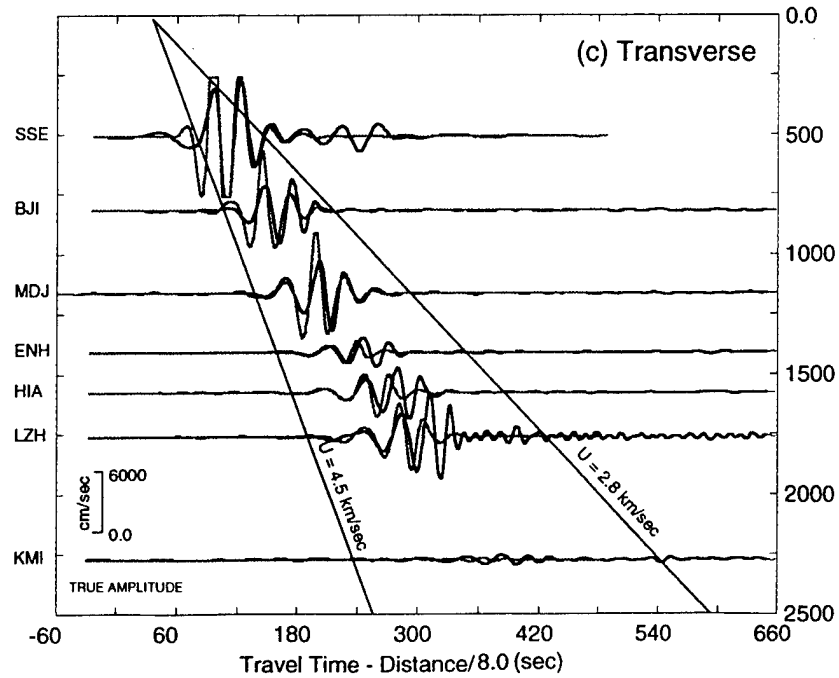
(c)

Figure 5. Vertical (a), Radial (b), and Transverse (c) Record Sections Comparing Observed Data (Solid Line) With Model A7 Synthetics (Dashed Line). The lines show the limits of the group velocity window between 4.5 and 2.8 km/sec.

(a)

(b)

Figure 6. Vertical (a), Radial (b), and Transverse (c) Record Sections for Model A8 Synthetics (Dashed Line) Compared to Observed Data (Solid Line). The lines show the limits of the group velocity window between 4.5 and 2.8 km/sec.
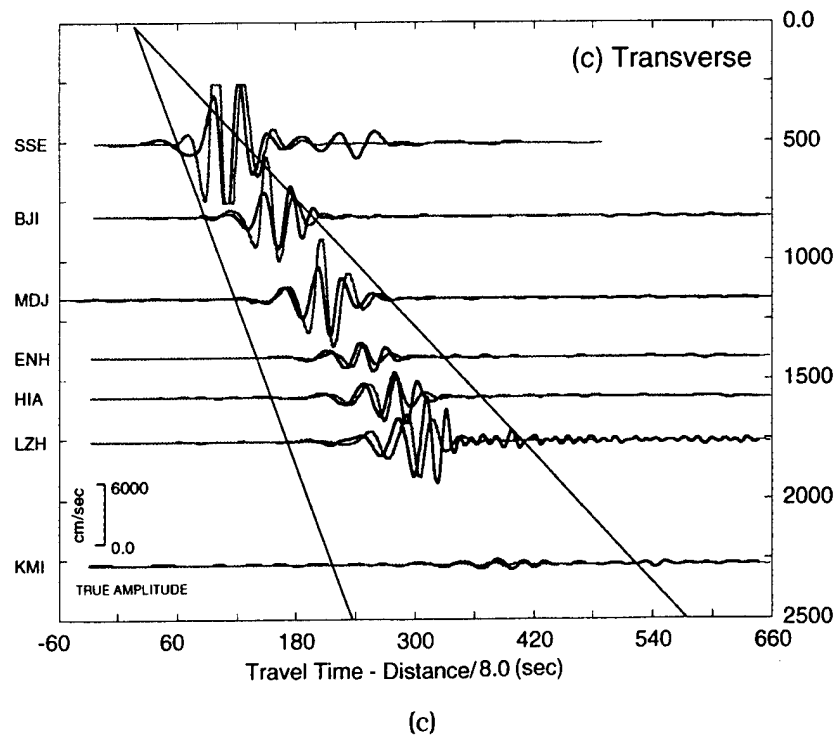
18

(c)

Figure 6. Vertical (a), Radial (b), and Transverse (c) Record Sections for Model A8 Synthetics (Dashed Line) Compared to Observed Data (Solid Line). The lines show the limits of the group velocity window between 4.5 and 2.8 km/sec.

7. CONCLUSIONS AND RECOMMENDATIONS

A grid search method has been implemented to determine earthquake focal mechanism and source depth using a set of Green's functions computed for a representative continental crustal structure. The method directly compares observed and synthetic waveforms through a misfit function, selecting as the result the model with the lowest misfit. The method has been tested with synthetic data and with CDSN long-period (LH band) observations of the 1992 Yellow Sea earthquake. I obtain a focal mechanism and source depth broadly consistent with that inferred by Nguyen (1994), although differing in details. Variations on the starting crustal model, which was derived from Nguyen and Hsu's (1993) MDJ model, are tested using the new focal mechanism. I find that better overall fits are obtained using higher attenuation throughout the crust and lower seismic velocity in the lower crust.

The inversions shown in this report were made using the LH channel of the CDSN stations. While this data set minimized the influence of small changes in crustal structure on the inversion, the long-period nature of the data precluded greater resolution of source depth and focal mechanism. In subsequent work, I plan to use this grid search algorithm with higher frequency seismograms computed from the broad-band (BH) signals. A convenient way to achieve higher frequency, yet interpretable, signals is to convolve the BH seismograms with the WWSSN 15-100 response. While this response is that of a real

19

instrument, it can be thought of as merely another filter. Its value lies in the fact that it is a causal filter and represents a well-known instrument type. We can bootstrap from the present study because model A8 can be used to compute the Green's functions for the fundamental fault types. A further extension of this work is to use model A8 as a generic crustal model for inverting regional waveform data from other parts of the world.

References

Cheng, Chiung-Chuan and Mitchell, Brian J. (1981) Crustal Q structure in the United States from multi-mode surface waves, *Bull. Seism. Soc. Am.*, **71**:161-181.

Fuchs, K. and Muller, G. (1971) Computation of synthetic seismograms with the reflectivity method and comparison with observations, *Geophys. J. Roy. Astron. Soc.*, **23**: 417-433.

Helmberger, D. V. and Engen, G.R. (1980) Modeling the long-period body waves from shallow earthquakes at regional distances, *Bull. Seism. Soc. Am.*, **70**:1699-1714.

Mangino, Stephen and Ebel, John (1992) *The Receiver Structure Beneath the Chinese Digital Seismograph Network (CDSN) Stations: Preliminary Results*, PL-TR-92-2149, Phillips Laboratory, Hanscom AFB, MA, ADA256681.

Menke, William (1984) *Geophysical Data Analysis: Discrete Inverse Theory*, Academic Press, 260pp.

Meissner, Rolf (1986) *The Continental Crust - A Geophysical Approach*, Academic Press, 426pp.

Muller, G. (1985) The reflectivity method: a tutorial, *J. Geophys.*, **58**:153-174.

Nguyen, Bao V. (1994) Surface-Wave focal mechanism of the 03 November 1992 Yellow-Sea main shock, *EOS (Trans. Am. Geophys. Union)*, **75**:241.

Nguyen, Bao V. and Hsu, Vindell (1993) Shear path structures from inversions of surface waves of the 03 November 1992 Yellow-Sea Main shock, *EOS (Trans. Am. Geophys. Union)*, **74**:426.

Peterson, J. and Tilgner, E.E. (1985) *Description and preliminary testing of the CDSN seismic sensor systems*, USGS Open File report 83-288, 37pp.

Wallace, Terry C., Helmberger, Donald V. and Mellman, George R. (1981) A technique for the inversion of regional data in source parameter studies, *J. Geophys. Res.*, **86**:1679-1685.

Zhao, Lian-She and Helmberger, Donald V. (1994) Source estimation from broadband regional seismograms, *Bull. Seism. Soc. Am.*, **84**:91-104.